

Low-rank surrogate modeling and stochastic zero-order optimization for training of neural networks with black-box layers

Andrei Chertkov^{a,b,*}, Artem Basharin^{a,b,*}, Mikhail Saygin^c, Evgeny Frolov^{a,b}, Stanislav Straupe^c, Ivan Oseledets^{a,b}

^a*Artificial Intelligence Research Institute (AIRI), Moscow, Russia*

^b*Skolkovo Institute of Science and Technology, Moscow, Russia*

^c*Sber Quantum Technology Center, Moscow, Russia*

Abstract

The growing demand for energy-efficient, high-performance AI systems has led to increased attention on alternative computing platforms (e.g., photonic, neuromorphic) due to their potential to accelerate learning and inference. However, integrating such physical components into deep learning pipelines remains challenging, as physical devices often offer limited expressiveness, and their non-differentiable nature renders on-device backpropagation difficult or infeasible. This motivates the development of hybrid architectures that combine digital neural networks with reconfigurable physical layers, which effectively behave as black boxes. In this work, we present a framework for the end-to-end training of such hybrid networks. This framework integrates stochastic zeroth-order optimization for updating the physical layer's internal parameters with a dynamic low-rank surrogate model that enables gradient propagation through the physical layer. A key component of our approach is the implicit projector-splitting integrator algorithm, which updates the lightweight surrogate model after each forward pass with minimal hardware queries, thereby avoiding costly full matrix reconstruction. We demonstrate our method across diverse deep learning tasks, including: computer vision (deep convolutional network on the CIFAR-10 dataset), audio classification (ECAPA-TDNN model on the UrbanSound8K dataset), and language modeling (a decoder-only transformer model on the FineWeb corpus). No-

*Equal contribution.

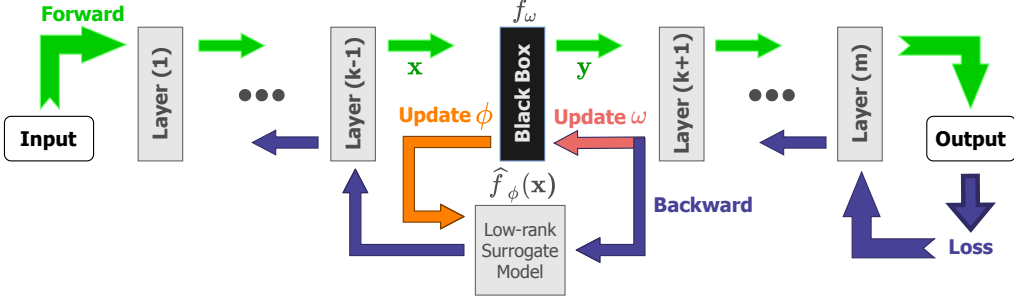


Figure 1: Schematic representation of the proposed method *astralora*.

table, across all modalities, the proposed approach achieves near-digital baseline accuracy and consistently enables effective end-to-end training of hybrid models incorporating various non-differentiable physical components (spatial light modulators, microring resonators, and Mach-Zehnder interferometers). This work bridges hardware-aware deep learning and gradient-free optimization, thereby offering a practical pathway for integrating non-differentiable physical components into scalable, end-to-end trainable AI systems.

Keywords: low-rank approximation, zeroth-order methods, surrogate modeling, hardware-aware training, photonic neural networks.

1. Introduction

Computational and energy demands of modern deep learning systems are rapidly outpacing the capabilities of conventional digital hardware [1]. This has intensified interest in alternative, non-von Neumann computing paradigms capable of providing faster and more energy-efficient machine learning. Among these, photonic systems offer a particularly promising path toward high-throughput, low-latency, and energy-efficient operation [2].

While photonic systems have demonstrated great potential for accelerating inference [3, 4, 5], leveraging them during training remains an open challenge [6, 7, 8]. Linear photonic systems [9, 10], capable of high-speed matrix-vector multiplication (MVM), are currently more mature and practical than their nonlinear counterparts [11, 12], which tend to remain inefficient and challenging to scale. However, the integration of even these linear components into deep learning pipelines introduces a set of non-trivial problems.

Most notably, photonic hardware is inherently non-differentiable, often

lacks precise programmability, and can exhibit issues such as noise, drift, or limited control resolution. These factors render standard backpropagation inapplicable, thereby limiting the ability to train such systems end-to-end. Moreover, the limited expressiveness of linear photonic models further complicates their direct deployment as plug-in replacements for entirely digital layers. Taken together, these challenges underscore the critical need for hybrid training pipelines that can effectively combine the raw speed of physical layers with the flexibility of digital deep learning frameworks. This motivates a central research question for this work:

How can we enable efficient, end-to-end training of a hybrid digital-physical neural network when critical components are black boxes, without access to their internal gradients or a pre-calibrated digital twin?

In this work, we introduce a novel approach *astralora* (Adaptive Surrogate TRAining with LOw RAnk) for training deep neural networks that incorporate a black-box linear photonic layer.¹ This layer is treated as a non-differentiable matrix-vector multiplication oracle: $f_{\omega}(\mathbf{x}) = A_{\omega}\mathbf{x}$. Here, the matrix A (representing the linear operation) depends on the physical layer’s parameters ω in a complex, non-explicit manner. To address the challenges of end-to-end training, we propose a two-part solution, schematically represented in Figure 1: a dynamically refined low-rank surrogate model $\hat{f}_{\phi}(\mathbf{x}) \approx f_{\omega}(\mathbf{x})$, which is computationally efficient and enables gradient flow through upstream layers; and a stochastic zeroth-order optimization scheme to update the internal, non-differentiable parameters ω , given that gradients with respect to ω are unavailable. Our method employs a parameter-disentangled surrogate $\hat{f}_{\phi}(\mathbf{x})$, which is trained online using a modified (implicit) projector-splitting integrator (PSI) algorithm [13]. This surrogate is computationally efficient and readily updated during training, thereby enabling efficient large-scale optimization even with photonic modules incorporated into the system.

We evaluate our approach through extensive experiments, employing deep convolutional models for machine vision and speech recognition tasks. Additionally, we conduct a more complex experiment utilizing a GPT-2-like architecture for a next-token prediction task, where feed-forward blocks are re-

¹A neural network may contain multiple physical layers, but for simplicity we assume the presence of a single such layer in the subsequent discussion without loss of generality.

placed with black-box photonic layers. Despite relying on approximate surrogate models and zeroth-order updates, our method demonstrates near-parity with fully differentiable baselines across various non-differentiable physical layers (e.g., spatial light modulators, microring resonators, and Mach-Zehnder interferometers). This crucial finding indicates that accurate backpropagation is not strictly required for successful end-to-end training in such hybrid systems. The main contributions of our work can be summarized as follows:

- We propose the implicit projector-splitting integrator (I-PSI) scheme, which enables efficient online retraining of low-rank surrogate models with minimal queries to a non-differentiable (black-box) physical layer.
- We develop the *astralora* framework, which successfully integrates non-differentiable physical layers into deep learning architectures through a synergistic combination of stochastic zeroth-order optimization and a dynamically updated surrogate model.
- We conduct comprehensive experimental validation² of our approach across three domains: image classification, audio classification, and large-scale language modeling, which demonstrates consistent effectiveness across diverse modalities for multiple types of physical layers.

2. Method

In our problem formulation (see Figure 1), we consider replacing the k -th linear layer of a deep neural network (NN) with a black box (BB) acting as a function:³

$$\mathbf{y} = f_{\omega}(\mathbf{x}) = A_{\omega}\mathbf{x}, \quad \mathbf{x} \in \mathbb{R}^{d_{inp}}, \quad \mathbf{y} \in \mathbb{R}^{d_{out}}, \quad \omega \in \mathbb{R}^{d_{bb}}, \quad A_{\omega} \in \mathbb{R}^{d_{out} \times d_{inp}}, \quad (1)$$

where \mathbf{x} is the input vector coming from the previous $(k - 1)$ th layer, \mathbf{y} is the output vector coming to the next $(k + 1)$ th layer, ω is the set of BB parameters, and A_{ω} is the matrix corresponding to the BB’s linear operation. Modern deep NNs fundamentally rely on automatic differentiation (autograd) and backpropagation for efficient training. To effectively leverage gradient-based optimization methods, it is necessary to compute the partial derivative

²The code for the *astralora* framework and all numerical examples from this work are publicly available in the repository <https://github.com/AndreiChertkov/astralora>.

³For brevity, the layer index is omitted in the subsequent formula for the BB action.

$\partial\mathcal{L}/\partial w$ of the loss function \mathcal{L} with respect to each parameter $w \in \Omega$, where Ω denotes the complete set of parameters in the NN. This process, in turn, requires the computation of two types of derivatives for each layer $f_{\omega^{(i)}}^{(i)}$ ($i = 1, 2, \dots, m$) in the NN: $\partial f_{\omega^{(i)}}^{(i)}/\partial \omega^{(i)}$ for updating the layer's parameters, and $\partial f_{\omega^{(i)}}^{(i)}/\partial \mathbf{x}^{(i)}$ for propagating gradients through the layer.

To update the parameters of the BB (refer to the “Train” stage in Figure 1), we employ a Monte-Carlo estimation method based on stochastic finite differences, detailed in Section 2.1. To pass the gradient through the BB during backpropagation (refer to the “Backward” stage in Figure 1) we utilize a low-rank surrogate model (SM) defined as:

$$\mathbf{y} = \hat{f}_\phi(\mathbf{x}) = USV^T \mathbf{x}, \quad U \in \mathbb{R}^{d_{out} \times r}, \quad S \in \mathbb{R}^{r \times r}, \quad V \in \mathbb{R}^{d_{inp} \times r}. \quad (2)$$

The parameters of the SM, denoted as $\phi = \{U, S, V\} \in \mathbb{R}^{d_{sm}}$, correspond to a rank- r decomposition of the BB matrix: $A_\omega \approx USV^T$. Following each training step, the SM parameters ϕ are updated using the I-PSI algorithm, as detailed in Section 2.2. Consequently, in Section 2.3, we present the *astralora* framework, which integrates non-differentiable physical layers into deep NNs.

2.1. Gradient estimation for the black-box layer

To update the parameters of the BB, we require the ability to calculate the action of the gradient operator (i.e., the gradient-vector product), denoted as $\mathbf{g}(\mathbf{x}, \mathbf{v})$. This operator acts on an arbitrary error vector $\mathbf{v} \in \mathbb{R}^{d_{out}}$, which originates from the subsequent layer during the backpropagation stage:

$$\mathbf{g}(\mathbf{x}, \mathbf{v}) = \left(\frac{\partial f_\omega(\mathbf{x})}{\partial \omega} \right)^\top \mathbf{v}.$$

This expression can alternatively be formulated as the partial derivative of the scalar product:

$$\mathbf{g}(\mathbf{x}, \mathbf{v}) = \frac{\partial}{\partial \omega} \langle f_\omega(\mathbf{x}), \mathbf{v} \rangle.$$

Given the unavailability of derivative for f_ω with respect to ω , we approximate the gradient using a stochastic finite-difference method. Specifically, we employ a well-known formula for the stochastic derivative (e.g., from [14]):

$$\mathbf{g}(\mathbf{x}, \mathbf{v}) \approx \frac{1}{\mu} \mathbb{E}_u (\langle f_{\omega+\mu u}(\mathbf{x}), \mathbf{v} \rangle - \langle f_\omega(\mathbf{x}), \mathbf{v} \rangle) = \frac{1}{\mu} \mathbb{E}_u \langle f_{\omega+\mu u}(\mathbf{x}) - f_\omega(\mathbf{x}), \mathbf{v} \rangle,$$

where $\mathbf{u} \in \mathbb{R}^{d_{bb}}$ is a random perturbation vector, typically sampled from a standard normal distribution ($\mathbf{u} \sim \mathcal{N}(0, 1)$), and $\mu > 0$ is a scalar magnitude parameter. For a practical approximation, the expectation $\mathbb{E}_{\mathbf{u}}$ is estimated using M_{BB} ($M_{BB} \geq 1$) random samples, leading to the following Monte Carlo approximation for the stochastic derivative:

$$\mathbf{g}(\mathbf{x}, \mathbf{v}) \approx \frac{1}{\mu \cdot M_{BB}} \sum_{i=1}^{M_{BB}} \langle f_{\omega+\mu\mathbf{u}_i}(\mathbf{x}) - f_{\omega}(\mathbf{x}), \mathbf{v} \rangle. \quad (3)$$

It is important to note that this formula necessitates $M_{BB} + 1$ queries to the BB for each derivative evaluation. The minimum number of samples M_{BB} required to ensure sufficient training accuracy for the entire NN, as well as the optimal scalar magnitude μ for the stability of derivative estimates, are determined empirically.

2.2. Update of the surrogate model while training

Following each training step, as the BB parameters evolve to ω_{new} , it becomes necessary to update the low-rank surrogate model (SM) \hat{f} , to maintain alignment with $f_{\omega_{new}}$. A naive approach would involve re-initializing the surrogate model, which typically entails computing (either exactly or approximately) the full matrix A_{ω} from the BB and subsequently performing a Singular Value Decomposition (SVD). However, this approach is impractical due to significant computational overhead, much of which cannot be efficiently offloaded to optical hardware. To address this challenge, we propose an extended version of the projector-splitting integrator (PSI) [13, 15], called the implicit PSI (I-PSI), which is presented in Algorithm 1. This algorithm enables efficient online updating of the low-rank SM with minimal queries to the BB hardware. The core insight is that, rather than reconstructing the entire matrix A_{ω} , we can efficiently update the existing low-rank decomposition by leveraging the incremental change $\Delta A = A_{\omega_1} - A_{\omega_0}$ between consecutive parameter updates.

The I-PSI algorithm proceeds in four key stages. First, it computes $P_1 = \Delta A V_0$ by evaluating the BB on the r columns of the current V matrix, which requires r queries to the BB. Second, it updates the left singular vectors by computing U_1 through QR decomposition of $K_1 = U_0 S_0 + P_1$, followed by a necessary correction to maintain the low-rank structure. Third,

Algorithm 1 Implicit projector-splitting integrator (I-PSI).

Require: function f_{ω} , that computes BB values; rank- r factor matrices U_0 , S_0 , V_0 of the current SM; weights of the BB before update ω_0 ; weights of the BB after update ω_1 ; number of allowed requests to the BB M_{sm}

Ensure: factor matrices U_1 , S_1 , V_1 of the updated SM

- 1: // Compute $P_1 = \Delta A V_0$ by querying the BB:
- 2: **for** $j \leftarrow 1$ to r **do**
- 3: $\mathbf{v}_j \leftarrow V[:, j]$
- 4: $\mathbf{p}_j \leftarrow f_{\omega_1}(\mathbf{v}_j) - f_{\omega_0}(\mathbf{v}_j)$
- 5: **end for**
- 6: $P_1 \leftarrow [\mathbf{p}_1, \mathbf{p}_2, \dots, \mathbf{p}_r]$
- 7: // Compute U_1 :
- 8: $K_1 \leftarrow U_0 S_0 + P_1$
- 9: $[U_1, \tilde{S}_0] \leftarrow \text{qr}(K_1)$
- 10: $\hat{S}_0 \leftarrow \tilde{S}_0 - U_1^\top P_1$
- 11: // Compute $P_2 = (\Delta A)^\top U_1$ using (4) and querying the BB:
- 12: **for** $j \leftarrow 1$ to M_{sm} **do**
- 13: $\mathbf{z}_j \leftarrow \mathcal{N}(0, 1)$
- 14: $\mathbf{p}_j \leftarrow \mathbf{z}_j (f_{\omega_1}(\mathbf{z}_j) - f_{\omega_0}(\mathbf{z}_j))^\top U$
- 15: **end for**
- 16: $P_2 \leftarrow \sum_{j=1}^{M_{sm}} \mathbf{p}_j$
- 17: // Compute V_1 :
- 18: $L_1 \leftarrow V_0 \hat{S}_0^\top + P_2$
- 19: $[V_1, S_1^\top] \leftarrow \text{qr}(L_1)$
- 20: $S_1 \leftarrow (S_1^\top)^\top$
- 21: **return** U_1, S_1, V_1

it approximates $P_2 = (\Delta A)^\top U_1$ using a stochastic projection method:

$$(\Delta A)^\top U \approx \sum_{i=1}^{M_{sm}} \mathbf{z}_i (\Delta A \mathbf{z}_i)^\top U, \quad \mathbf{z}_i \sim \mathcal{N}(0, 1), \quad (4)$$

where $\mathbf{z}_i \in \mathbb{R}^{d_{inp}}$ is a random normal vector. This step requires M_{sm} random probes to approximate the transpose action without direct access to $(\Delta A)^\top$. Finally, it updates the right singular vectors by computing V_1 through QR decomposition of $L_1 = V_0 \hat{S}_0^\top + P_2$.

This approach is particularly well-suited for BB components for several

critical reasons. First, it exclusively requires forward evaluations of the BB, not gradient information, thus making it directly applicable to physical components such as photonic layers that inherently cannot provide gradient feedback. Second, it achieves significant query efficiency: the total query complexity⁴ is $2r + 2M_{sm}$, which is substantially lower than the $O(d_{out} \cdot d_{inp})$ queries typically required for full matrix reconstruction. Third, it enables online adaptation by incrementally updating the existing SM rather than rebuilding it from scratch, thereby efficiently leveraging prior information to maintain accuracy. It is notable that the theoretical foundations of the projector-splitting approach ensure numerical stability during updates while preserving the manifold structure of rank- r matrices. This property is crucial for maintaining the low-rank constraint throughout the training process. Empirically, we observe that even with relatively small values of r and moderate query budgets M_{sm} , the SM remains sufficiently accurate to enable effective gradient propagation through the NN, as demonstrated by our experimental results in Section 5.

2.3. The proposed approach *astralora*

Bringing together the steps, described in the previous sections, we summarize the comprehensive training flow in Algorithm 2. During the forward pass, the BB layer performs the actual physical computation. Conversely, the SM is utilized during backpropagation to approximate gradients, as the BB itself is non-differentiable. The BB parameters are updated via stochastic finite-difference queries. Subsequently, after each update, the SM is efficiently realigned with the new BB state using the I-PSI algorithm. Thus, *astralora* seamlessly integrates gradient-free optimization and surrogate modeling into a single, coherent training pipeline, and the central advantage is its query efficiency. Our approach enables an efficient trade-off between the number of BB queries and the gradient approximation error. This contrasts with conventional finite-difference-based schemes, which typically require a fixed $O(b \cdot d_{inp})$ queries (where b is the batch size) for error propagation through a black-box layer.

While initially motivated by photonic hardware, the *astralora* scheme is not exclusively restricted to optical systems. Indeed, any non-differentiable

⁴Algorithm 1 requires $2r$ queries for matrix-vector products and $2M_{sm}$ queries for matrix-transpose-vector products. For simplicity in discussing the update budget during numerical experiments, we will refer just to M_{sm} .

Algorithm 2 The training step with *astralora*.

Require: training data batch (\mathbf{x}, \mathbf{y}) ; digital parameters θ ; function f_ω , that computes BB values; BB parameters ω ; initial SM factors $\phi = \{U, S, V\}$; learning rates for digital parameters η , and for BB parameters η_{BB} ; perturbation scale μ ; query budgets M_{BB} , and M_{SM} ; loss function \mathcal{L}

Ensure: updated θ_1 , ω_1 , and ϕ_1

- 1: // **Forward pass:**
- 2: $\mathbf{x}_{in} \leftarrow \text{NN}_{\text{before}}(\mathbf{x})$ \triangleright Compute input to BB layer
- 3: $\mathbf{y}_{bb} \leftarrow f_\omega(\mathbf{x}_{in})$ \triangleright Query the physical BB layer
- 4: $\hat{\mathbf{y}} \leftarrow \text{NN}_{\text{after}}(\mathbf{y}_{bb})$ \triangleright Compute output of the NN
- 5: $\mathcal{L} \leftarrow \mathcal{L}(\hat{\mathbf{y}}, \mathbf{y})$ \triangleright Compute the loss
- 6: // **Backward pass:**
- 7: $\mathbf{v} \leftarrow \nabla_{\mathbf{y}_{bb}} \mathcal{L}$ \triangleright Gradient from downstream layers via autograd
- 8: $\mathbf{g}_{in} \leftarrow VS^\top U^\top \mathbf{v}$ \triangleright Approximate gradient w.r.t. BB input using SM
- 9: $\nabla_\theta \mathcal{L} \leftarrow \text{Backpropagate}(\mathbf{g}_{in})$ \triangleright Propagate through upstream layers
- 10: // **Update:**
- 11: $\theta_1 \leftarrow \theta - \eta \cdot \nabla_\theta \mathcal{L}$ \triangleright Update digital parameters via SGD
- 12: $\mathbf{g}_\omega(\mathbf{x}, \mathbf{v}) \approx \frac{1}{\mu \cdot M_{BB}} \sum_{i=1}^{M_{BB}} \langle f_{\omega+\mu \mathbf{u}_i}(\mathbf{x}) - f_\omega(\mathbf{x}), \mathbf{v} \rangle$ \triangleright See Section 2.1
- 13: $\omega_1 \leftarrow \omega - \eta_{bb} \cdot \text{mean}_{\mathbf{x}}(\mathbf{g}_\omega)$ \triangleright Zeroth-order update for BB parameters
- 14: $\phi_1 \leftarrow \text{I-PSI}(f_\omega, \phi, \omega, \omega_1, M_{sm})$ \triangleright Update SM (see Algorithm 1)

or hardware-constrained module, including neuromorphic accelerators, analogue chips, or other black-box hardware can, in principle, be integrated into a trainable NN using the same strategy. This positions *astralora* as a general framework for hybrid digital–physical learning. In the subsequent sections, we demonstrate that *astralora* enables end-to-end training across diverse tasks and physical layer implementations, consistently achieving accuracy comparable to fully digital baselines while maintaining query efficiency.

3. Related work

End-to-end training of neural networks with non-differentiable black-box layers presents inherent challenges, primarily because traditional backpropagation cannot propagate gradients through such components. This section reviews relevant prior work essential to our approach. We begin by examining gradient-free optimization methods, which, while enabling optimization without explicit gradients, commonly suffer from significant inefficiency at scale.

Next, we discuss low-rank approximation techniques, typically employed to accelerate gradient-based learning in fully differentiable models. We highlight their inapplicability to true black-box systems, as they rely on an explicitly differentiable matrix. Finally, we survey existing training approaches for physical neural networks, noting that these often lack efficient and truly joint optimization strategies across their hybrid digital-physical components. Our proposed *astralora* framework directly addresses these limitations by synergistically combining stochastic zeroth-order optimization with a dynamically updated low-rank surrogate model, thereby facilitating gradient propagation through otherwise non-differentiable components.

3.1. Gradient-free methods for neural networks

Backpropagation relies on gradient calculations derived via automatic differentiation, which can encounter challenges when dealing with discontinuous, noisy, or non-differentiable objective functions. Gradient-free (zeroth-order, or ZO) methods offer viable alternatives, trading computational efficiency for increased robustness to irregular loss surfaces and the ability to optimize non-differentiable components. Below, we discuss several works that have proposed approaches to improve the performance of ZO methods when applied to modern LLMs.

The work [16] pioneered variance-reduced ZO for nonconvex problems, mitigating the high sample complexity of classical ZO methods through accelerated stochastic gradient estimators. Their key innovation integrates a variance reduction technique with two-point gradient estimators to minimize black-box functions. While the method is validated effectively on black-box tasks like adversarial attacks and material classification, it remains fundamentally query-inefficient for high-dimensional NN training due to its reliance on iterative forward-pass sampling for gradient approximation, requiring $O(d)$ queries per epoch, where d is the dimensionality.

The authors of [17] addressed memory constraints with MeZO (memory-efficient zeroth-order optimizer), enabling the fine-tuning of billion-parameter LLMs using only forward passes. By employing simultaneous perturbation stochastic approximation (SPSA) with in-place perturbation resampling, MeZO achieves a memory footprint equivalent to inference while maintaining performance competitive with backpropagation. However, MeZO’s primary focus on fine-tuning pre-trained models limits its applicability to end-to-end training of networks containing non-differentiable components, as its convergence relies heavily on pre-trained initializations and task prompts.

The work [18] proposes LOZO, a memory-efficient ZO optimization method for fine-tuning language models that exploits low-rank gradient structures. By approximating gradients via low-rank perturbation matrices (LGE) and employing lazy subspace sampling, LOZO captures intrinsic gradient properties while avoiding the need for activation storage. We note that while LOZO reduces memory overhead for full-model ZO optimization, it lacks mechanisms for localized gradient approximation within non-differentiable components.

The recent work [19] addresses the memory bottleneck in large RNN training by replacing backpropagation through time (BPTT) with Central-Difference Random Gradient Estimation (CD-RGE). Their method approximates gradients via forward-pass perturbations, eliminating intermediate activation storage and reducing VRAM requirements, thereby enabling billion-parameter RNN training on single GPUs. While effective for homogeneous RNNs achieving up to $19\times$ faster convergence than BPTT, their approach requires hundreds of perturbation steps per update, incurring prohibitive computational overhead for systems with slow physical components. Furthermore, CD-RGE treats the entire model as a black box, making it difficult to propagate the gradient to upstream layers.

Discussion. In summary, while recent advances in ZO have improved memory efficiency and scalability for fine-tuning LLMs, critical gaps persist for the end-to-end training of hybrid architectures containing non-differentiable layers. Variance-reduced methods like [16] suffer from prohibitive $O(d)$ query complexity in high dimensions. Meanwhile, memory-efficient optimizers such as MeZO [17] and LOZO [18] rely on pre-trained initializations and lack mechanisms for localized gradient propagation through individual black-box modules. Although LOZO exploits low-rank structures for memory reduction, its monolithic gradient estimator cannot backpropagate signals upstream of non-differentiable components. Similarly, CD-RGE [19] incurs excessive computational overhead for physical systems and treats the entire model as a single black box. Our work bridges these gaps by introducing a dynamic low-rank surrogate framework that enables efficient, layer-wise gradient approximation. By emulating non-differentiable layers with lightweight linear surrogates after each forward pass, we achieve localized gradient propagation to upstream layers; online retraining capability without pre-training dependencies; and rank-constrained efficiency that avoids $O(d)$ sampling. This approach uniquely supports the end-to-end optimization of systems integrat-

ing physical components while scaling to hundreds of millions of parameters, which is a key advantage over existing ZO methods.

3.2. Low-rank approximation for backpropagation

Low-rank approximation techniques have emerged as powerful tools to address computational and memory bottlenecks in backpropagation-based training of deep NNs. By exploiting intrinsic low-dimensional structures in weight matrices or gradient updates, these methods enable the efficient training of large-scale models while maintaining performance. This subsection reviews key approaches leveraging low-rank representations to optimize gradient-based learning, focusing on their reliance on end-to-end differentiability, which is a fundamental constraint that limits their applicability in systems containing non-differentiable components.

Authors of [20] propose LoRA-GA, an enhanced initialization scheme for Low-Rank Adaptation (LoRA) that accelerates convergence through gradient alignment (GA). The core innovation involves initializing low-rank adapter matrices U and V using SVD of the full-model gradient matrix ($\nabla_A \mathcal{L}$). This ensures that the first optimization step of the low-rank product UV closely approximates the direction of full fine-tuning gradients, i.e., $\Delta(UV) \approx \zeta \Delta A$, where A is a matrix of weights. Empirical validation shows LoRA-GA achieves 2-4 \times faster convergence than vanilla LoRA. However, the approach fundamentally relies on explicit gradient computation through all layers during initialization (via SVD of $\nabla_A \mathcal{L}$), making it incompatible with architectures containing non-differentiable black-box components.

Similarly, the recent work [21] proposes Gradient Low-Rank Projection (GaLore), a memory-efficient training strategy for LLMs. GaLore leverages the intrinsic low-rank structure of gradients during optimization to reduce the memory consumption of optimizer. Unlike LoRA, which constrains weight updates to a static low-rank subspace, GaLore performs full-parameter learning through dynamic low-rank projections of gradients. While GaLore offers substantial improvements in memory efficiency for several LLMs, it remains constrained by its reliance on end-to-end differentiability.

The work [22] addresses memory constraints in on-device training through low-rank gradient approximation. By reparameterizing weight gradients as $\nabla \mathcal{L}(A) \approx U \nabla \mathcal{L}(V)^\top + \nabla \mathcal{L}(U) V^\top$ (where U and V are low-rank factors), the authors effectively leverage low-rank structure in gradient space rather than weight space, preserving model capacity while enabling memory-intensive

optimizers on resource-limited devices. We note that this method fundamentally relies on differentiable operations and backpropagation-compatible components. This constitutes a significant limitation for our target scenario involving non-differentiable black-box modules (e.g., physical components) where gradients become inaccessible.

The study in [23] proposes using forward gradients with locally supervised auxiliary losses to approximate backpropagation, replacing random directional derivatives with local network gradients to reduce variance. While effective for standard architectures (e.g., reducing ResNet-18’s accuracy gap from $\sim 40\%$ to $\sim 3\%$ on CIFAR-10), their method fundamentally assumes differentiability throughout the computational graph and requires architectural modifications to inject auxiliary networks at intermediate layers.

Recent work [24] introduces AdaRankGrad, a method that exploits the empirical observation that gradient matrices in LLM training exhibit progressively lower rank. Their approach adaptively projects gradients onto low-rank subspaces during Adam optimization, reducing memory usage by 25-50% while maintaining performance. We note that while effective for differentiable networks, AdaRankGrad fundamentally relies on backpropagation-compatible layers. However, the empirical observation regarding the low rank of gradients in this work is certainly very interesting in the context of our method.

Follow-up work [25] proposes SUMO, a subspace-aware optimizer that leverages exact SVD-based orthogonalization of first-order moments within dynamically adapted low-rank subspaces to accelerate memory-efficient LLM training. By explicitly aligning optimization steps with spectral loss landscape characteristics, SUMO mitigates approximation errors from iterative methods like Newton-Schulz orthogonalization. It theoretically bounds these errors and demonstrates empirically faster convergence with 20% memory reduction compared to other methods (e.g., GaLore) in both pre-training and fine-tuning scenarios. We note that SUMO assumes gradient-based moment updates, which prevents direct application of this approach to NNs containing black-box components.

Discussion. While the reviewed methods demonstrate compelling advantages in memory efficiency and convergence acceleration for differentiable NNs, they fundamentally depend on end-to-end gradient propagation. This renders them inapplicable when black-box components (e.g., physical layers) disrupt the computational graph. Our approach overcomes this limitation through

two synergistic innovations. First, we replace explicit gradient calculations at non-differentiable layers with a lightweight, dynamically updated low-rank surrogate model that enables continuous gradient approximation to upstream layers. Second, we decouple black-box parameter optimization using stochastic zeroth-order methods, eliminating differentiability requirements downstream. Crucially, our framework maintains the computational benefits of low-rank representations (similar to methods like GaLore and LoRA-GA) but extends them to hardware-aware scenarios where physical components introduce non-differentiable operations. The dual strategy of surrogate modeling and gradient-free optimization establishes a new paradigm for end-to-end trainable systems that remains tractable even at scale. This addresses a critical gap not resolved by existing low-rank approximation techniques.

3.3. Training approaches for physical neural networks

Photonic NNs in particular, and analog NNs in general are typically trained by one of three complementary routes, supported by a growing software stack. First, many systems rely on calibrated digital surrogates and chip-in-the-loop updates: a “digital twin” is fitted offline and then mapped to hardware, with measurements used to compensate for mismatch. A representative example is [26], which trains with a well-calibrated surrogate and then deploys weights to the chip. For scalable on-chip adaptation, [27] propose state calibration, analytical zeroth-order core mapping, and subspace learning with multi-level sparsity to maintain efficient in-situ updates. When true gradients are difficult to access, zeroth-order training can still be effective at scale; e.g., [28] show variance-reduced, tensor-compressed ZO updates that are useful for hardware-aware optimization. Ideas from the edge computing community, while electronic, can be adopted conceptually for photonics. E.g., [29] constrain updates to a subset of parameters for memory and latency efficiency during continual adaptation.

Second, in-situ gradient methods enable the training of photonic NNs without resorting to the calculation of derivatives in the digital electronic domain. This is achieved by propagating the learning signal through the same optical circuits themselves. The first experimental demonstration of in-situ backpropagation on a reconfigurable silicon-photonics mesh is presented in [30], which exploits bidirectional propagation and internal taps to measure gradients and perform updates largely on-chip. For diffractive free-space systems, the theoretical framework for optical adjoints was proposed

in [31]. An alternative that keeps both passes in optics is the end-to-end optical backpropagation, analyzed by [32], which leverages saturable-absorber nonlinearities and pump-probe dynamics. A closely related milestone is a single-chip photonic deep NN trained with forward-only updates [33].

Third, backpropagation-free, forward-only training algorithms avoid reverse-mode physics entirely and can be robust to nonidealities. Direct Feedback Alignment replaces symmetric weight transport with fixed random feedback and has been demonstrated in the hybrid electro-photonic training of modern architectures [34]. The Forward–Forward algorithm [35] optimizes per-layer “goodness” over positive and negative examples; building on this algorithmic proposal, an optical realization is reported in [36]. For hardware where gradients are inaccessible or excessively noisy, Multiplexed Gradient Descent (MGD) offers fast ZO updates via multiplexed perturbations [37].

These methods are enabled by an expanding software ecosystem for differentiable photonics and cross-layer co-design: Neurophox [38] for unitary/orthogonal meshes and ONN simulation; Photontorch [39] for PyTorch-native photonic circuit simulation with autograd; PyTorch-ONN [40] for coherent/incoherent ONN layers at scale; SimPhony (ScopeX-ASU) [41] for device-circuit-architecture co-modeling; and DAT MPNN [42] as a reference implementation of Dual Adaptive Training.

Discussion. While photonic and analog NNs benefit from multiple complementary training paradigms, each exhibits limitations that constrain end-to-end optimization. Digital-surrogate methods reliably map software-trained models to hardware but require careful calibration and incur overhead for in-situ adaptation, thereby limiting scalability. In-situ gradient approaches allow direct gradient propagation on optical circuits, yet they depend on specific architectures and on-chip measurement infrastructure, making them less flexible. Backpropagation-free, forward-only algorithms offer robustness under inaccessible or noisy gradients, but their convergence and generalization performance can be architecture-dependent and often lag behind gradient-based methods for complex tasks. While the growing software ecosystem facilitates simulation, co-design, and hybrid training, no existing approach fully addresses scalability, hardware variability, and training efficiency simultaneously. Our work aims to bridge these gaps by introducing flexible, hardware-aware surrogate methods that enable localized gradient propagation, efficient online adaptation, and integration of non-differentiable photonic components in large-scale architectures.

4. Simulated physical layers

This section characterizes the physical photonic devices that constitute the black-box (BB) layers within our hybrid modeling framework. We investigate five distinct architectures: generic programmable matrix-vector multiplier (MVM); spatial light modulator (SLM) for dynamic wavefront shaping; microring resonator (MRR) banks for wavelength-selective operations; structured matrix layer based on Monarch matrices and SLM blocks, and Mach-Zehnder interferometers (MZIs).

Each layer is characterized by a transfer matrix A_{ω} that maps an input vector \mathbf{x} to an output vector, expressed as $f_{\omega}(\mathbf{x}) = A_{\omega}\mathbf{x}$. The relationship between A_{ω} and the tunable parameters ω varies across different models, reflecting the diversity of optical hardware implementations. Consequently, our training approach is evaluated with layers whose transfer matrices range from straightforward to highly intricate functions of ω . A more detailed description of each layer under consideration⁵ is provided below.

4.1. Matvec layer

A particularly straightforward linear optical layer is one whose transfer-matrix elements can be programmed independently and directly. In this case, the trainable weights ω are mapped onto the matrix

$$A_{\omega}^{(matvec)} = \text{reshape}(\omega, (d_{out}, d_{inp})), \quad (5)$$

as in cross-bar-programmable photonic circuits [43]. We refer to this configuration as the “matvec” layer because, while it behaves like a conventional digital matrix–vector multiplication, it is still trained purely as a BB.

4.2. MRR layer

In integrated photonics, using microring resonators (MRRs) provides a convenient way of manipulating optical fields in a compact and energy-efficient settings. Therefore, optical multipliers exploiting programmable MRRs, such as MRR weight banks are considered as one of the architecture of linear layers for NNs [44]. The MRR linear layer, which we used in our simulations, is shown in Figure 2A and operates as follows. First, the

⁵For all considered layers, an additional scalar scale parameter is included (trained gradiently), as the elements of the matrix A_{ω} have limited values for some layers.

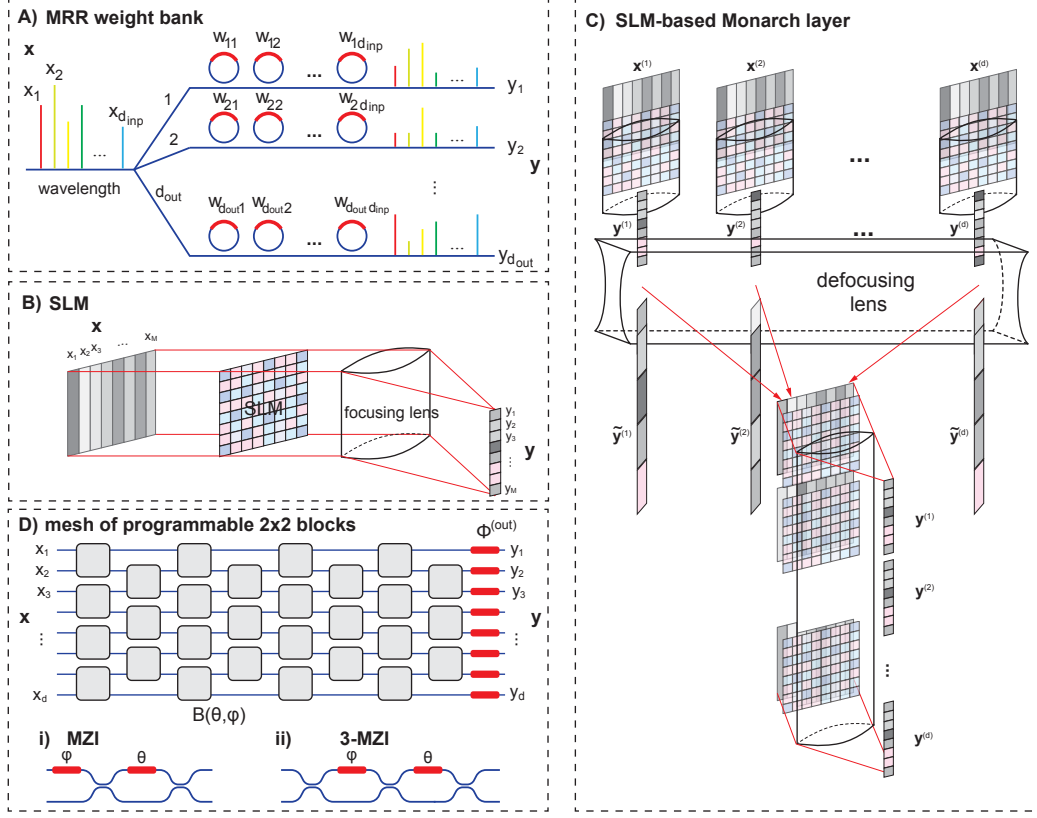


Figure 2: Illustration of the physical layers simulated in this work: a) MRR weight banks, b) SLM-based multiplier, c) Monarch matrix multiplier exploiting SLM-based optical blocks, d) planar interferometric meshes of the MZI (i) and 3-MZI (ii) blocks.

input vector $\mathbf{x} = (x_1, x_2, \dots, x_{d_{inp}})$ is encoded onto a set of optical carriers with centre wavelengths λ_j , so that the optical field amplitude at wavelength λ_j equals the corresponding vector element x_j . These spectral components are then fanned out into d_{out} parallel waveguides, each evanescently coupled to a separate row of MRRs.

The k -th row contains d_{inp} resonators. Each resonator multiplies one component x_j by its programmed weight A_{kj} . The value of A_{kj} is set by tuning the phase-shift value w_{kj} of the corresponding MRR in the bank, such that $A_{kj} = \text{func}(w_{kj})$, where function looks like

$$\text{func}(w) = 2 \sqrt{\frac{a^2 + r^2 - 2ar \cos w}{1 + (ar)^2 - 2ar \cos w}} - 1. \quad (6)$$

Here, a and r are the intrinsic amplitude transmission and self-coupling coefficients of the MRR, which depend on the physical implementation of the layer. In our experiments, we used representative values $a = 0.8$ and $r = 0.9$.

After modulation, the weighted optical fields in each row are coherently summed, yielding the desired operation. Overall, the layer implements the linear transformation

$$A_{\omega}^{(MRR)} = \text{reshape}(\text{func}(\omega), (d_{out}, d_{inp})). \quad (7)$$

4.3. SLM layer

Free-space optics provides access to a high-dimensional parameter space, making it well-suited for massively parallel information processing. It enables linear operations using optical components such as lenses and spatial modulators. In this work, we consider two optical layers implemented via free-space optics.

The simplest free-space MVM scheme, illustrated in Figure 2B, was first proposed in [45] and later implemented for reconfigurable large-scale algebraic operations in [32]. This optical arrangement utilizes a spatial light modulator (SLM) combined with a cylindrical lens. The SLM comprises a 2D array of programmable pixels capable of modulating the phase profile of an incoming optical beam. The phase shift values represent the trainable weights of the linear layer.

To multiply an input real-valued vector \mathbf{x} by a $d_{out} \times d_{inp}$ matrix $A_{\omega}^{(SLM)}$, the input vector is encoded as d_{inp} optical field amplitudes with corresponding amplitude values x_i ($i = 1, 2, \dots, d_{inp}$). Each amplitude is spatially expanded vertically to overlap with corresponding columns of SLM pixels, each column having a size of d_{out} . A cylindrical lens then focuses the optical field horizontally onto a narrow vertical slit. In this dimension, the lens performs a Fourier transform, and the slit selects only the zero spatial frequency component. Immediately after the slit, the complex optical fields are described by:

$$z_j = \frac{1}{\sqrt{d_{inp}}} \sum_{i=1}^{d_{inp}} e^{i\theta_{ji}} x_i, \quad (8)$$

where $\theta_{ji} = \text{reshape}(\omega, (d_{out}, d_{inp}))$ represents the real phase shifts applied by the SLM. Assuming measurement of the real components of the optical fields z_j , we define the output as $y_j = \text{Re}(z_j)$ for $j = 1, 2, \dots, d_{out}$. Thus, the

transfer matrix of the SLM layer is given by:

$$A_{\omega}^{(SLM)} = \frac{1}{\sqrt{d_{inp}}} \text{reshape}(\cos \omega, (d_{out}, d_{inp})). \quad (9)$$

4.4. SLM Monarch layer

The second free-space layer is inspired by digital Monarch matrices, which are structured matrices designed as parameter-efficient and expressive alternatives to dense linear layers [46, 47]. A Monarch matrix is defined by the product $PLP^T R$, where P is a permutation matrix transforming from row-major to column-major ordering, and L and R are block-diagonal matrices given by: $L = \bigoplus_{\beta=1} L^{(\beta)}$, $R = \bigoplus_{\gamma=1} R^{(\gamma)}$, where β and γ mark the blocks within the block-diagonals.

The corresponding optical implementation, inspired by the block structure of Monarch matrices, is depicted in Figure 2C. This implementation leverages multiple SLM-based MVM setups for block matrix multiplication. However, our optical Monarch layer deviates from traditional digital Monarch matrices due to the complex-valued matrices L and R attainable with free-space optics. Moreover, to facilitate multiplication by non-square matrices, the block matrices $L^{(\beta)}$ and $R^{(\gamma)}$ can be rectangular, having dimensions $n_L^{(out)} \times n_L^{(inp)}$ and $n_R^{(out)} \times n_R^{(inp)}$, respectively. The block dimensions relate directly to the provided input and output sizes d_{inp} and d_{out} . These dimensions are decomposed into products of two nearest powers of two: $d_{inp} = b_R n_R^{(inp)}$, $d_{out} = b_L n_L^{(out)}$, where b_R and b_L indicate the number of blocks within matrices R and L , respectively. The remaining dimensions are determined by matching the output dimension of R to the input dimension of L , resulting in $n_R^{(out)} = b_L$ and $n_L^{(inp)} = b_R$.

The resulting output of the optical Monarch layer is:

$$y_{jl} = \text{Re} \left(\sum_{i=1}^{b_1} L_{ji}^{(l)} \sum_{k=1}^{n_1^{(inp)}} R_{lk}^{(i)} \right) \mathbf{x}_{ik}, \quad j = 1, \dots, n_2^{(out)}; l = 1, \dots, b_2, \quad (10)$$

with $R_{lk}^{(i)} = \frac{1}{\sqrt{n_1^{(inp)}}} e^{i\theta_{lk}^{(R)}}$ and $L_{ji}^{(l)} = \frac{1}{\sqrt{n_2^{(out)}}} e^{i\theta_{ji}^{(L)}}$. As in the simpler SLM layer, the phase shifts $\theta_{lk}^{(R)}$ and $\theta_{ji}^{(L)}$ constitute the trainable weights ω of the optical Monarch layer.

4.5. Planar programmable meshes

Another our model of the optical layers describes the programmable interferometer circuits proposed in [48] and [49]. Such programmable circuits are widely used in classical and quantum information processing [50]. These circuits have the form of planar meshes consisting of 2×2 blocks $B(\theta, \varphi)$, each of which is independently programmed by tunable phase-shifts θ and φ . We consider two types of blocks, namely, the Mach-Zehnder interferometer (MZIs) and 3-splitter MZI (3-MZI), depicted in Figure 2D (i) and (ii), respectively. Each MZI is parametrized by independent angles θ and φ specified by the adjustable phase-shifts. The MZI and 3-MZI block transforms the incoming amplitudes according to the transfer matrices:

$$B_{\text{MZI}}(\theta, \varphi) = e^{i\theta/2} \begin{pmatrix} e^{i\varphi} \sin(\theta/2) & \cos(\theta/2) \\ e^{i\varphi} \cos(\theta/2) & -\sin(\theta/2) \end{pmatrix},$$

$$B_{\text{3MZI}}(\theta, \varphi) = \frac{e^{i\frac{\varphi+\theta}{2}}}{\sqrt{2}} \begin{pmatrix} -\cos \frac{\theta-\varphi}{2} + i \sin \frac{\theta+\varphi}{2} & -\sin \frac{\theta-\varphi}{2} + i \cos \frac{\theta+\varphi}{2} \\ \sin \frac{\theta-\varphi}{2} + i \cos \frac{\theta+\varphi}{2} & -\cos \frac{\theta-\varphi}{2} - i \sin \frac{\theta+\varphi}{2} \end{pmatrix}.$$

Accordingly, the $N \times N$ transfer matrix is obtained as a multiplication of N MZI layers. Together with the angles of the output phase-shifts $\Phi^{(out)}$, the number of all angles parameterizing the 2×2 blocks sum up to N^2 , exactly the number of parameters to specify arbitrary $N \times N$ unitary matrices. These angle parameters are the trainable weights ω . To implement the MZI mesh layer with transfer matrices $A_{\omega}^{(MZI)}$ of arbitrary dimensions, we embed them into an N -mode interferometer with $N = \max(d_{out}, d_{inp})$ and make padding of the dangling inputs or outputs. We note that the dependence of $A^{(MZI)}(\omega)$ on trainable parameters is very nonlinear and much more complicated than that of the MRR weight bank or SLM-based layers.

5. Numerical experiments

To demonstrate the practical utility of our hybrid training framework, *astralora*, we conduct comprehensive experiments that integrate digital emulations of the photonic layers described in the previous section. These software-based models accurately replicate the input-output behavior and, crucially, the black-box parameter-to-matrix mapping of their physical counterparts (e.g., MRRs, SLMs, MZI meshes). This approach allows for controlled,

scalable validation of our framework without the experimental variability inherent to physical hardware. We emphasize that while the simulations themselves are computationally intensive, an actual photonic implementation would perform these operations without such a digital bottleneck. Our evaluation⁶ spans multiple domains: image classification, audio analysis, and text generation, confirming the framework’s adaptability to real-world constraints and its ability to maintain competitive accuracy across diverse tasks.

5.1. CIFAR-10 image classification

We validate our framework on the well-known CIFAR-10 image classification benchmark [51], using a deep convolutional neural network. The base architecture⁷ consists of three convolutional blocks with residual connections, followed by global average pooling. The final components are a classification block consisting of the primary linear layer (512×1024) and an output linear layer (1024×10). We replace the primary linear layer with one of our BB layers (“matvec”, “mrr”, “slm”, “monarch”, “mzi”, and “3-mzi”) and perform computations for various ranks r of the SM model and varying numbers of allowed requests to the BB during the update of its parameters (M_{bb}) and during the update of the SM parameters M_{sm} (for simplicity, we fix $M_{bb} = M_{sm} = M$). For all combinations of $r = 1, 3, 5, 7, 10, 50, 100$ and $M = 1, 10, 100, 1000$, we perform the computation five times for different random seeds and report the average result along with its boundary values in Figure 3. For comparison, we also show the training result for the original model (referred to as the “Digital” curve) without replacing layers, trained with standard gradient-based optimization. Results demonstrate that all photonic layer types achieve near-digital accuracy when sufficient rank ($r \geq 10$) and hardware queries ($M \geq 100$) are used, thus validating the effectiveness of the *astralora* framework for training NNs with physical black-box components.

⁶We note that the digital emulation of the MZI mesh’s transfer function (“mzi” and “3-mzi” layers) is computationally expensive, rendering training prohibitively slow for our large-scale experiments. Therefore, we exclude them from the audio classification and text generation tasks, but present results for the simpler task of image classification.

⁷Our pipeline is based on the repository <https://github.com/KellerJordan/cifar10-airbench>.

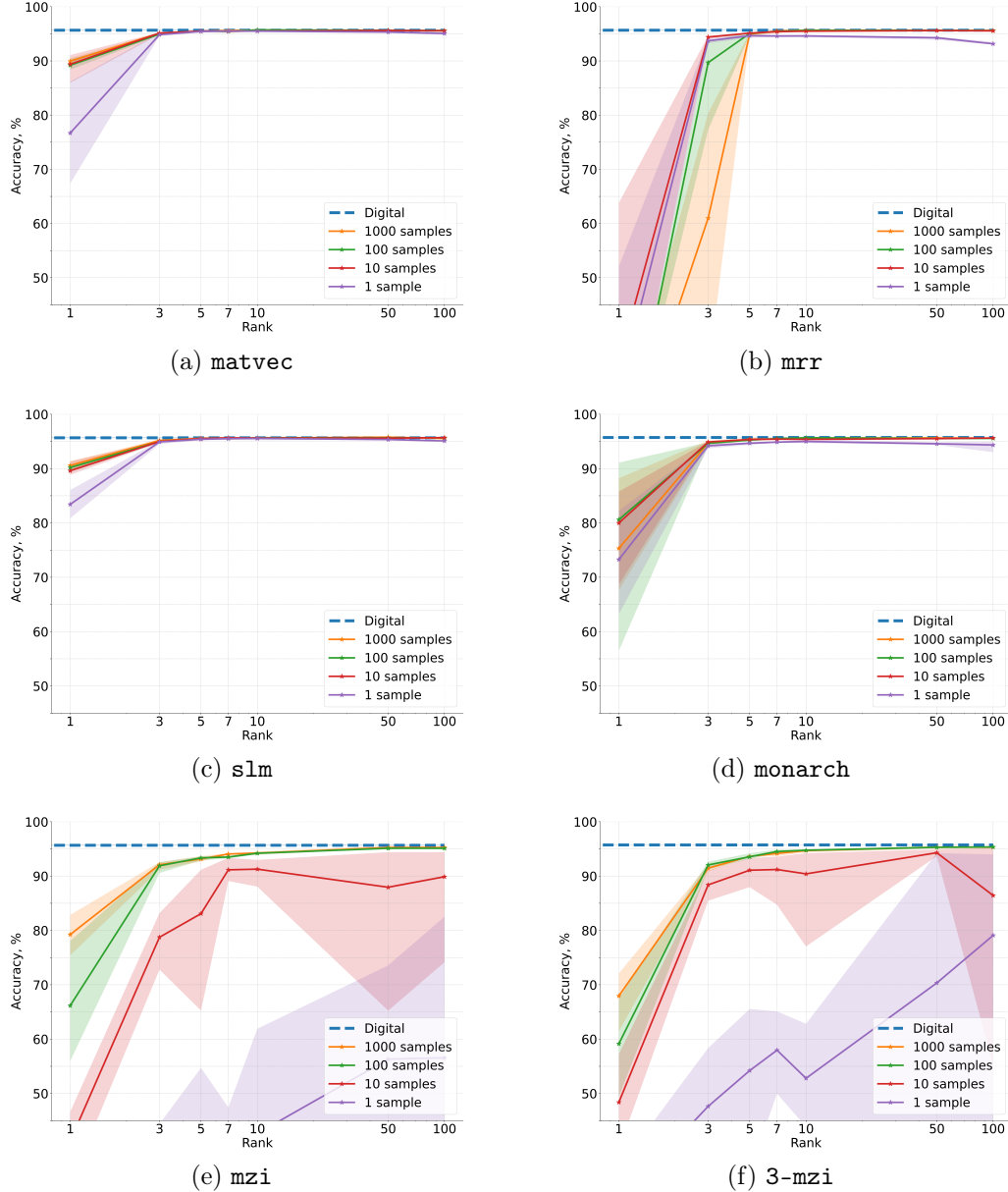


Figure 3: Accuracy results averaged over five independent runs for CIFAR-10 image classification using a deep convolutional neural network architecture where one linear layer is replaced with non-differentiable physical photonic layer.

Table 1: Accuracy results (%) for the audio classification problem using the UrbanSound8K dataset with the ECAPA-TDNN architecture. We consider different ranks of the SM and four BB layer types. All results are averaged over five independent runs. Reference accuracy of the digital model is 78.50%.

Rank of the SM	Accuracy (%)			
	matvec	mrr	slm	monarch
1	72.25	65.60	70.49	40.99
5	76.88	72.47	75.28	76.25
10	77.22	77.07	77.94	77.68
50	77.63	75.53	77.78	78.18
100	78.38	76.53	77.89	79.75

5.2. Audio classification problem

We further test our framework on the audio classification problem using the UrbanSound8K dataset [52] with the ECAPA-TDNN architecture [53]⁸. This problem presents unique challenges due to the temporal nature of audio data and the need for precise feature extraction. To simulate hardware integration, we replace a critical component in the ECAPA-TDNN feature extractor, i.e., the linear layer (6144×192), with a BB layer while maintaining the original channel dimensions. We fix $M_{bb} = M_{sm} = 1000$ and perform the training for different rank values $r = 1, 5, 10, 50, 100$. The results are averaged over five independent runs and reported in the Table 1.

The results demonstrate the consistent effectiveness of the *astralora* framework across diverse physical layer implementations (“matvec”, “mrr”, “slm”, and “monarch”) for the audio classification task. All four tested black-box layer types successfully converged, achieving final accuracy within 1 – 2% of the fully digital baseline (78.50%) when a sufficient surrogate rank ($r \geq 10$) was used. This narrow performance gap highlights that accurate gradient propagation, rather than exact backpropagation, is sufficient for effective end-to-end training. We observe that the more complex, hardware-realistic layers (“mrr”, “slm”, “monarch”) initially lag behind the idealized “matvec” layer at very low ranks ($r = 1, 5$) but rapidly close this gap as the rank

⁸Our pipeline is based on the repository <https://github.com/speechbrain/speechbrain>.

increases. Notably, the “monarch” layer, with its inherently structured design, achieves the highest performance at rank 100, even slightly surpassing the digital baseline, suggesting its architectural inductive bias is particularly well-suited to this task. These findings confirm that our method is not only viable but also robust to the specific nonlinearities and parameter-to-matrix mappings imposed by different hardware platforms.

5.3. Large-scale language modeling

To rigorously validate the scalability and robustness of our framework, we conducted large-scale language modeling experiments using a GPT-2-like architecture (417M parameters) [54]⁹ trained on a subset of the FineWeb dataset [55]. This task presents a formidable challenge due to the model’s size, the complexity of the natural language data, and the need for precise gradient approximations across multiple non-differentiable components.

We designed two distinct stress tests. In the first experiment (Table 2), we replaced only the first linear layer (of size 1536×6144) within one or more MLP blocks. The blocks targeted for replacement were selected starting from the end of the network; thus, replacing one block means modifying the last MLP block, replacing four blocks modifies the last four, and so on. This setup isolates the impact of introducing a black-box layer into the linear transformation part of the MLP.

In the second, more ambitious experiment (Table 3), we replaced entire MLP blocks with black-box equivalents. Here both linear layers and the intermediate nonlinearity within the block were treated as a single, monolithic black-box component. Again, replacement proceeded from the end of the network. This scenario tests the framework’s ability to handle a much more complex and deeply non-differentiable function.

For both experiments, we fixed the query budgets to $M_{bb} = 100$ for parameter updates and $M_{sm} = 1000$ for surrogate model refinement. The results, presented in Tables 2 and 3, demonstrate the consistent effectiveness of the *astralora* framework. In both setups, we observe a graceful degradation in performance as the number of replaced components increases. This is expected, as each black-box layer introduces a small approximation error in the gradient. The fact that the network remains trainable even when

⁹Our pipeline is based on the repository <https://github.com/KellerJordan/modded-nanogpt>.

Table 2: Validation perplexity for the language modeling with GPT-2-like architecture on FineWeb dataset with 1, 4, 8, and 12 linear layers in MLP blocks replaced by BB.

# of replaced layers	# of digital parameters	Perplexity			
		matvec	mrr	slm	monarch
0	$417M$			23.80	
1	$408M$	24.04	24.28	24.04	24.28
4	$379M$	25.02	25.27	25.02	25.02
8	$342M$	26.84	27.11	26.84	27.11
12	$304M$	30.26	30.87	30.26	30.56

Table 3: Validation perplexity for the language modeling with GPT-2-like architecture on FineWeb dataset with 1, 4, 8, and 12 MLP blocks replaced by BB.

# of replaced blocks	# of digital parameters	Perplexity			
		matvec	mrr	slm	monarch
0	$417M$		23.80		
1	$398M$	24.28	25.02	24.28	24.53
4	$342M$	25.02	25.53	25.27	25.02
8	$266M$	27.11	28.50	27.11	28.21
12	$190M$	31.18	31.50	30.87	32.13

12 entire blocks are replaced (reducing the number of digitally updated parameters from $417M$ to $190M$) is a strong testament to the robustness of our approach. We also note that the performance is remarkably consistent across all four physical layer types (“matvec”, “mrr”, “slm”, and “monarch”), highlighting the general applicability of our method.

6. Conclusions

In this work, we introduce *astralora*, a general framework for training hybrid neural networks that incorporate non-differentiable physical components such as photonic layers. By coupling stochastic zeroth-order optimization for hardware parameter updates with a dynamically refined low-rank surrogate model for gradient propagation, *astralora* enables efficient end-to-end optimization without reliance on task-specific heuristics or restrictive

architectural modifications. Our implicit projector-splitting integrator ensures lightweight surrogate updates with minimal hardware queries, effectively bridging the gap between physical device constraints and the demands of modern deep learning pipelines.

Extensive experiments across computer vision, speech recognition, and large-scale language modeling confirm that *astralora* consistently achieves near-digital baseline accuracy, demonstrating its robustness across diverse modalities and physical implementations. These results clearly highlight that accurate backpropagation is not strictly necessary for training hybrid networks with non-differentiable layers, provided efficient surrogate strategies are successfully employed. Overall, *astralora* provides a practical route for embedding physical layers into AI systems, thereby contributing toward the long-term goal of hardware-aware, energy-efficient, and high-performance machine learning.

References

- [1] I. H. Sarker, Deep learning: a comprehensive overview on techniques, taxonomy, applications and research directions, *SN computer science* 2 (6) (2021) 1–20.
- [2] I. Bente, S. Taheriniya, F. Lenzini, F. Brückerhoff-Plückelmann, M. Kues, H. Bhaskaran, C. D. Wright, W. Pernice, The potential of multidimensional photonic computing, *Nature Reviews Physics* (2025) 1–12.
- [3] M. Moralis-Pegios, G. Mourgias-Alexandris, A. Tsakyridis, G. Gi-amougiannis, A. Totovic, G. Dabos, N. Passalis, M. Kirtas, T. Ruti-rawut, F. Gardes, et al., Neuromorphic silicon photonics and hardware-aware deep learning for high-speed inference, *Journal of Lightwave Technology* 40 (10) (2022) 3243–3254.
- [4] S.-Y. Ma, T. Wang, J. Laydevant, L. G. Wright, P. L. McMahon, Quantum-limited stochastic optical neural networks operating at a few quanta per activation, *Nature Communications* 16 (1) (2025) 359.
- [5] S. R. Ahmed, R. Baghdadi, M. Bernadskiy, N. Bowman, R. Braid, J. Carr, C. Chen, P. Ciccarella, M. Cole, J. Cooke, et al., Universal photonic artificial intelligence acceleration, *Nature* 640 (8058) (2025) 368–374.

- [6] B. J. Shastri, A. N. Tait, T. Ferreira de Lima, W. H. Pernice, H. Bhaskaran, C. D. Wright, P. R. Prucnal, Photonics for artificial intelligence and neuromorphic computing, *Nature Photonics* 15 (2) (2021) 102–114.
- [7] K. Liao, T. Dai, Q. Yan, X. Hu, Q. Gong, Integrated photonic neural networks: Opportunities and challenges, *ACS Photonics* 10 (7) (2023) 2001–2010.
- [8] A. Montes McNeil, Y. Li, A. Zhang, M. Moebius, Y. Liu, Fundamentals and recent developments of free-space optical neural networks, *Journal of Applied Physics* 136 (3) (2024).
- [9] M. Moralis-Pegios, G. Giamougiannis, A. Tsakyridis, D. Lazovsky, N. Pleros, Perfect linear optics using silicon photonics, *Nature Communications* 15 (1) (2024) 5468.
- [10] A. Najjar Amiri, A. D. Vit, K. Gorgulu, E. S. Magden, Deep photonic network platform enabling arbitrary and broadband optical functionality, *Nature Communications* 15 (1) (2024) 1432.
- [11] M. Yildirim, N. U. Dinc, I. Oguz, D. Psaltis, C. Moser, Nonlinear processing with linear optics, *Nature Photonics* 18 (10) (2024) 1076–1082.
- [12] H. Wang, J. Hu, A. Morandi, A. Nardi, F. Xia, X. Li, R. Savo, Q. Liu, R. Grange, S. Gigan, Photonics breakthroughs 2024: Nonlinear photonic computing at scale, *IEEE Photonics Journal* (2025).
- [13] C. Lubich, I. V. Oseledets, A projector-splitting integrator for dynamical low-rank approximation, *BIT Numerical Mathematics* 54 (1) (2014) 171–188.
- [14] A. Chen, Y. Zhang, J. Jia, J. Diffenderfer, J. Liu, K. Parasyris, Y. Zhang, Z. Zhang, B. Kailkhura, S. Liu, Deepzero: Scaling up zeroth-order optimization for deep model training, *arXiv preprint arXiv:2310.02025* (2023).
- [15] O. Olaleke, I. Oseledets, E. Frolov, Dynamic modeling of user preferences for stable recommendations, in: *Proceedings of the 29th ACM Conference on User Modeling, Adaptation and Personalization*, 2021, pp. 262–266.

- [16] S. Liu, B. Kailkhura, P.-Y. Chen, P. Ting, S. Chang, L. Amini, Zeroth-order stochastic variance reduction for nonconvex optimization, *Advances in neural information processing systems* 31 (2018).
- [17] S. Malladi, T. Gao, E. Nichani, A. Damian, J. D. Lee, D. Chen, S. Arora, Fine-tuning language models with just forward passes, *Advances in Neural Information Processing Systems* 36 (2023) 53038–53075.
- [18] Y. Chen, Y. Zhang, L. Cao, K. Yuan, Z. Wen, Enhancing zeroth-order fine-tuning for language models with low-rank structures, *arXiv preprint arXiv:2410.07698* (2024).
- [19] F. Chaubard, M. Kochenderfer, Scaling recurrent neural networks to a billion parameters with zero-order optimization, *arXiv preprint arXiv:2505.17852* (2025).
- [20] S. Wang, L. Yu, J. Li, Lora-ga: Low-rank adaptation with gradient approximation, *Advances in Neural Information Processing Systems* 37 (2024) 54905–54931.
- [21] J. Zhao, Z. Zhang, B. Chen, Z. Wang, A. Anandkumar, Y. Tian, Galore: Memory-efficient llm training by gradient low-rank projection, *arXiv preprint arXiv:2403.03507* (2024).
- [22] M. Gooneratne, K. C. Sim, P. Zadrazil, A. Kabel, F. Beaufays, G. Motta, Low-rank gradient approximation for memory-efficient on-device training of deep neural network, in: *ICASSP 2020-2020 IEEE International Conference on Acoustics, Speech and Signal Processing (ICASSP)*, IEEE, 2020, pp. 3017–3021.
- [23] L. Fournier, S. Rivaud, E. Belilovsky, M. Eickenberg, E. Oyallon, Can forward gradient match backpropagation?, in: *International Conference on Machine Learning*, PMLR, 2023, pp. 10249–10264.
- [24] Y. Refael, J. Svirsky, B. Shustin, W. Huleihel, O. Lindenbaum, Adarankgrad: Adaptive gradient-rank and moments for memory-efficient llms training and fine-tuning, *arXiv preprint arXiv:2410.17881* (2024).

- [25] Y. Refael, G. Smorodinsky, T. Tirer, O. Lindenbaum, SUMO: Subspace-aware moment-orthogonalization for accelerating memory-efficient LLM training, arXiv preprint arXiv:2505.24749 (2025).
- [26] T. Fu, Y. Zang, Y. Huang, Z. Du, H. Huang, C. Hu, M. Chen, S. Yang, H. Chen, Photonic machine learning with on-chip diffractive optics, *Nature Communications* 14 (1) (2023) 70.
- [27] J. Gu, H. Zhu, C. Feng, Z. Jiang, R. Chen, D. Pan, L2ight: Enabling on-chip learning for optical neural networks via efficient in-situ subspace optimization, in: M. Ranzato, A. Beygelzimer, Y. Dauphin, P. Liang, J. W. Vaughan (Eds.), *Advances in Neural Information Processing Systems*, Vol. 34, Curran Associates, Inc., 2021, pp. 8649–8661.
- [28] Y. Zhao, X. Yu, Z. Chen, Z. Liu, S. Liu, Z. Zhang, Tensor-compressed back-propagation-free training for (physics-informed) neural networks (2023).
- [29] Z. Qu, Z. Zhou, Y. Tong, L. Thiele, p-meta: Towards on-device deep model adaptation, in: *Proceedings of the 28th ACM SIGKDD Conference on Knowledge Discovery and Data Mining*, KDD '22, ACM, 2022, p. 1441–1451.
- [30] S. Pai, Z. Sun, T. W. Hughes, T. Park, B. Bartlett, I. A. D. Williamson, M. Minkov, M. Milanizadeh, N. Abebe, F. Morichetti, A. Melloni, S. Fan, O. Solgaard, D. A. B. Miller, Experimentally realized in situ backpropagation for deep learning in photonic neural networks, *Science* 380 (6643) (2023) 398–404.
- [31] T. Zhou, L. Fang, T. Yan, J. Wu, Y. Li, J. Fan, H. Wu, X. Lin, Q. Dai, In situ optical backpropagation training of diffractive optical neural networks, *Photon. Res.* 8 (6) (2020) 940–953.
- [32] J. Spall, X. Guo, T. D. Barrett, A. I. Lvovsky, Fully reconfigurable coherent optical vector–matrix multiplication, *Opt. Lett.* 45 (20) (2020) 5752–5755.
- [33] S. Bandyopadhyay, A. Sludds, S. Krastanov, R. Hamerly, N. Harris, D. Bunandar, M. Streshinsky, M. Hochberg, D. Englund, Single-chip photonic deep neural network with forward-only training, *Nature Photonics* 18 (12) (2024) 1335–1343.

- [34] Z. Wang, K. Müller, M. Filipovich, J. Launay, R. Ohana, G. Pariente, S. Mokaadi, C. Brossollet, F. Moreau, A. Cappelli, I. Poli, I. Carron, L. Daudet, F. Krzakala, S. Gigan, Streamlined optical training of large-scale modern deep learning architectures with direct feedback alignment (2025).
- [35] G. Hinton, The forward-forward algorithm: Some preliminary investigations, arXiv preprint arXiv:2212.13345 2 (3) (2022) 5.
- [36] I. Oguz, J. Ke, Q. Weng, F. Yang, M. Yildirim, N. U. Dinc, J.-L. Hsieh, C. Moser, D. Psaltis, Forward-forward training of an optical neural network, *Opt. Lett.* 48 (20) (2023) 5249–5252.
- [37] A. N. McCaughan, B. G. Oripov, N. Ganesh, S. W. Nam, A. Dienstfrey, S. M. Buckley, Multiplexed gradient descent: Fast online training of modern datasets on hardware neural networks without backpropagation, *APL Machine Learning* 1 (2) (2023) 026118.
- [38] S. Pai, I. A. Williamson, T. W. Hughes, M. Minkov, O. Solgaard, S. Fan, D. A. Miller, Parallel fault-tolerant programming of an arbitrary feed-forward photonic network, arXiv preprint arXiv:1909.06179 (2019).
- [39] F. Laporte, J. Dambre, P. Bienstman, Highly parallel simulation and optimization of photonic circuits in time and frequency domain based on the deep-learning framework pytorch, *Scientific reports* 9 (1) (2019) 5918.
- [40] J. Gu, H. Zhu, C. Feng, Z. Jiang, R. T. Chen, D. Z. Pan, L2ight: Enabling on-chip learning for optical neural networks via efficient in-situ subspace optimization, in: *Conference on Neural Information Processing Systems (NeurIPS)*, 2021.
- [41] Z. Yin, M. Zhang, A. Begovic, R. Huang, J. Zhang, J. Gu, Simphony: A device-circuit-architecture cross-layer modeling and simulation framework for heterogeneous electronic-photonic ai system, arXiv preprint arXiv:2411.13715 (2024).
- [42] Z. Zheng, Z. Duan, H. Chen, R. Yang, S. Gao, H. Zhang, H. Xiong, X. Lin, Dual adaptive training of photonic neural networks, *Nature Machine Intelligence* (2023) 1–11.

- [43] G. Giampougiannis, A. Tsakyridis, Y. Ma, A. Totović, M. Moralis-Pegios, D. Lazovsky, N. Pleros, A coherent photonic crossbar for scalable universal linear optics, *Journal of Lightwave Technology* 41 (8) (2023) 2425–2442.
- [44] A. N. Tait, A. X. Wu, T. F. de Lima, E. Zhou, B. J. Shastri, M. A. Nahmias, P. R. Prucnal, Microring weight banks, *IEEE Journal of Selected Topics in Quantum Electronics* 22 (6) (2016) 312–325.
- [45] N. Tamura, J. C. Wyant, Two-dimensional matrix multiplication using coherent optical techniques, *Opt. Eng.* 18 (198) (1979).
- [46] T. Dao, B. Chen, N. Sohoni, A. Desai, M. Poli, J. Grogan, A. Liu, A. Rao, A. Rudra, C. Ré, Monarch: Expressive structured matrices for efficient and accurate training (2022).
- [47] S. Qiu, A. Potapczynski, M. Finzi, M. Goldblum, A. G. Wilson, Compute better spent: Replacing dense layers with structured matrices, *arXiv preprint arXiv:2406.06248* (2024).
- [48] W. R. Clements, P. C. Humphreys, B. J. Metcalf, W. S. Kolthammer, I. A. Walmsley, Optimal design for universal multiport interferometers, *Optica* 3 (12) (2016) 1460–1465.
- [49] R. Hamerly, S. Bandyopadhyay, D. Englund, Asymptotically fault-tolerant programmable photonics, *Nature Communications* 13 (1) (2022) 6831.
- [50] M. Dong, M. Zimmermann, D. Heim, H. Choi, G. Clark, A. J. Leenheer, K. J. Palm, A. Witte, D. Dominguez, G. Gilbert, M. Eichenfield, D. Englund, Programmable photonic integrated meshes for modular generation of optical entanglement links, *npj Quantum Information* 9 (1) (2023) 42.
- [51] A. Krizhevsky, G. Hinton, et al., Learning multiple layers of features from tiny images (2009).
- [52] J. Salamon, C. Jacoby, J. P. Bello, A dataset and taxonomy for urban sound research, in: *Proceedings of the 22nd ACM international conference on Multimedia*, 2014, pp. 1041–1044.

- [53] B. Desplanques, J. Thienpondt, K. Demuynck, ECAPA-TDNN: Emphasized channel attention, propagation and aggregation in tdnn based speaker verification, arXiv preprint arXiv:2005.07143 (2020).
- [54] A. Radford, J. Wu, R. Child, D. Luan, D. Amodei, I. Sutskever, et al., Language models are unsupervised multitask learners, OpenAI blog 1 (8) (2019) 9.
- [55] G. Penedo, H. Kydlíček, L. B. allal, A. Lozhkov, M. Mitchell, C. Raffel, L. V. Werra, T. Wolf, The fineweb datasets: Decanting the web for the finest text data at scale, in: The Thirty-eight Conference on Neural Information Processing Systems Datasets and Benchmarks Track, 2024.